

LEGUS DISCOVERY OF A LIGHT ECHO AROUND SUPERNOVA 2012AW

SCHUYLER D. VAN DYK¹, JANICE C. LEE², JAY ANDERSON², JENNIFER E. ANDREWS³, DANIELA CALZETTI⁴, STACEY N. BRIGHT², LEONARDO UBEDA², LINDA J. SMITH⁵, ELENA SABBÌ², EVA K. GREBEL⁶, ARTEMIO HERRERO^{7,8}, AND SELMA E. DE MINK⁹

To Appear in ApJ

ABSTRACT

We have discovered a luminous light echo around the normal Type II-Plateau Supernova (SN) 2012aw in Messier 95 (M95; NGC 3351), detected in images obtained approximately two years after explosion with the Wide Field Channel 3 on-board the *Hubble Space Telescope* (*HST*) by the Legacy ExtraGalactic Ultraviolet Survey (LEGUS). The multi-band observations span from the near-ultraviolet through the optical (F275W, F336W, F438W, F555W, and F814W). The apparent brightness of the echo at the time was ~ 21 – 22 mag in all of these bands. The echo appears circular, although less obviously as a ring, with an inhomogeneous surface brightness, in particular, a prominent enhanced brightness to the southeast. The SN itself was still detectable, particularly in the redder bands. We are able to model the light echo as the time-integrated SN light scattered off of diffuse interstellar dust in the SN environment. We have assumed that this dust is analogous to that in the Milky Way with $R_V = 3.1$. The SN light curves that we consider also include models of the unobserved early burst of light from the SN shock breakout. Our analysis of the echo suggests that the distance from the SN to the scattering dust elements along the echo is ≈ 45 pc. The implied visual extinction for the echo-producing dust is consistent with estimates made previously from the SN itself. Finally, our estimate of the SN brightness in F814W is fainter than that measured for the red supergiant star at the precise SN location in pre-SN images, possibly indicating that the star has vanished and confirming it as the likely SN progenitor.

Subject headings: dust, extinction — scattering — supernovae: general — supernovae: individual (SN 2012aw) — galaxies: individual (NGC 3351, Messier 95, M95)

1. INTRODUCTION

Light echoes from transient events provide a probe of both the circumstellar and interstellar structures in the environment (e.g., Crotts & Kunkel 1991; Xu et al. 1995), of the size distribution and chemical composition of the scattering dust (e.g., Sugerman 2003), and of the detailed history of the outburst giving rise to the echo (e.g., Rest et al. 2012b). Echoes also could provide a geometric distance to the event, independent of the distance ladder, through analysis of polarized light (Sparks 1994, 1996). A number of resolved light echoes have been discovered historically, including those of novae (Kapteyn 1901; Ritchey 1901; Sokoloski et al. 2013), unusual outbursting stars (Bond et al. 2003), erupting luminous blue

variables (Rest et al. 2012a; Prieto et al. 2014), and ancient Galactic and Local Group supernovae (SNe; Krause et al. 2005; Rest et al. 2005; Krause et al. 2008; Rest et al. 2008a,b). See Rest et al. (2012b) for a review. Although light echoes from more recent extragalactic SNe could well be a common occurrence, observations which spatially resolve echoes are relatively rare, with only 11 occurrences known in total, as summarized in Table 1. Inferences have been made for the existence of possible light echoes around a number of other SNe, mostly from reemission of SN light by dust in the infrared (Meikle et al. 2006; Welch et al. 2007; Mattila et al. 2008; Miller et al. 2010; Sugerman et al. 2012). The main obstacle to resolving the echo is that the SN host galaxies must be relatively nearby, although, even then, the structures can only be revealed by the superior angular resolution of the *Hubble Space Telescope* (*HST*).

The light echo of a SN results from the luminous ultraviolet (UV)/optical pulse scattered by dust in the SN environment. We essentially see a reflection of the event itself (Patat 2005). In particular, if the light echo is detected in the UV, we have a record of the bright, rapid flash of X-ray/UV emission emerging as the SN shock breaks through the massive envelope around the progenitor star (Crotts et al. 1992), an event that is elusive on account of its promptness and brevity (e.g., Quimby et al. 2007; Schawinski et al. 2008; Gezari et al. 2008, 2015). Much of the circumstellar matter and small dust grains nearest to the SN will be destroyed by the pulse, although more distant, larger grains will survive. The observed light echo at a particular instant in time is the

¹ IPAC/Caltech, Mailcode 100-22, Pasadena, CA 91125, USA; email: vandyk@ipac.caltech.edu.

² Space Telescope Science Institute, 3700 San Martin Drive, Baltimore, MD 21218, USA.

³ Steward Observatory, University of Arizona, Tucson, AZ 85721, USA.

⁴ Department of Astronomy, University of Massachusetts, Amherst, MA 01003, USA.

⁵ European Space Agency/Space Telescope Science Institute, Baltimore, MD 21218, USA.

⁶ Astronomisches Rechen-Institut, Zentrum für Astronomie der Universität Heidelberg, Mönchhofstr. 12-14, 69120 Heidelberg, Germany.

⁷ Instituto de Astrofísica de Canarias, Vía Láctea s/n, E-38200 La Laguna (S.C. Tenerife), Spain

⁸ Departamento de Astrofísica, Universidad de La Laguna, Avda. Astrofísico Francisco Sánchez s/n, E-38071 La Laguna (S.C. Tenerife), Spain

⁹ Anton Pannenkoek Astronomical Institute, University of Amsterdam, 1090 GE Amsterdam, The Netherlands

intersection of a dust sheet or filament with the (virtual) ellipsoid surface of constant arrival time, which results in nearly all cases as a circle or arc on the sky.

We have discovered a resolved light echo around the normal SN II-Plateau (II-P) 2012aw in the SB(r)b spiral host galaxy Messier 95 (M95; NGC 3351), during the course of the Legacy ExtraGalactic UV Survey (LEGUS; GO-13364, PI: D. Calzetti). LEGUS is a Cycle 21 *HST* Treasury Program which imaged 50 nearby ($\lesssim 12$ Mpc) galaxies in multiple bands with the Wide Field Camera 3 (WFC3) UVIS channel and the Advanced Camera for Surveys (ACS) Wide Field Channel. See Calzetti et al. (2015) for a detailed introduction to the survey. LEGUS particularly concentrated on obtaining images of these well-studied galaxies in the WFC3/UVIS F275W and F336W bands.

The SN has been extensively studied in the UV, optical, and near-infrared by Bayless et al. (2013), Bose et al. (2013), and Dall’Ora et al. (2014). Yadav et al. (2014) analyzed radio observations of the SN. The SN progenitor was identified in archival *HST* Wide-Field and Planetary Camera 2 (WFPC2) F555W and F814W and ground-based J and K_s images as a likely red supergiant (RSG) star by both Van Dyk et al. (2012) and Fraser et al. (2012). Both Fraser et al. and Van Dyk et al. found that the RSG was cool ($3500 \lesssim T_{\text{eff}}(\text{K}) \lesssim 4500$; although, Van Dyk et al. more narrowly limited T_{eff} to ≈ 3600 K), must have had a dusty circumstellar environment, and was therefore quite luminous ($L_{\star} \gtrsim 10^5 L_{\odot}$) and of relatively high initial mass¹⁰ ($M_{\text{ini}} \simeq 15\text{--}25 M_{\odot}$), based on the stellar evolutionary models from Eldridge et al. (2008) and Ekström et al. (2012), respectively. Kochanek et al. (2012) reanalyzed the data from both papers, employing a different approach for the treatment of the circumstellar extinction, and argued that the progenitor had to have been less luminous ($L_{\star} < 10^5 L_{\odot}$) and less massive ($M_{\text{ini}} < 15 M_{\odot}$). Van Dyk et al. (in preparation) have revisited the progenitor photometry and conclude that the star likely had $L_{\star} \approx 10^{4.9} L_{\odot}$ and $M_{\text{ini}} \approx 12 M_{\odot}$. Jerkstrand et al. (2014) modeled late-time spectra from the nebular phase and found that the emission lines from likely nucleosynthetic products indicate a progenitor initial mass in the range 14–18 M_{\odot} .

In this paper we describe the observations and analysis of the light echo and the ramifications for the properties of the SN and its progenitor. We assume a reddening- and metallicity-corrected distance modulus to the host galaxy of 30.00 ± 0.09 mag (measured using Cepheids; Freedman et al. 2001), which is a distance of 10.0 ± 0.4 Mpc. The inclination of M95 is relatively low, at 41° , with position angle 192° (Tamburro et al. 2008), so internal line-of-sight effects should be minimal. The SN occurred $58''.3$ W and $115''.8$ S of the host galaxy nucleus, in a region of the galaxy with no obvious signs of recent massive star formation. Bose et al. (2013) adopted 2012 March 16.1 (JD 2456002.6 \pm 0.8) as the time of the SN explosion. Dall’Ora et al. (2014) adopted March 16.0 (JD 2456002.5 \pm 0.8). These are essentially the same for the purposes of our analysis below. UT dates are used

¹⁰ This actually should be referred to as a “single-star-equivalent initial mass,” since the majority of massive stars is expected to exchange mass or merge with a binary companion before explosion (Sana et al. 2012).

TABLE 1
SPATIALLY RESOLVED SUPERNOVA LIGHT ECHOES^a

SN	Type	Host Galaxy	Distance (Mpc)	References
1987A	II-P	LMC	0.05	1,3,15
1991T	Ia	NGC 4527	15	9
1993J	IIb	M81	3.4	7,10
1995E	Ia	NGC 2441	49.6	8
1998bu	Ia	M96	9.9	2
2003gd	II-P	M74	10.0	11,12
2006X	Ia	M100	15.2	14
2007af	Ia	NGC 5584	23	5
2008bk	II-P	NGC 7793	3.4	13
2012aw	II-P	M95	10.0	16
2014J	Ia	M82	3.5	4

REFERENCES. — (1) Bond et al. (1990); (2) Cappellaro et al. (2001); (3) Crots (1988); (4) Crots (2014); (5) Drozdov et al. (2014); (6) Gouiffes et al. (1988); (7) Liu et al. (2003); (8) Quinn et al. (2006); (9) Sparks et al. (1999); (10) Sugerman & Crots (2002); (11) Sugerman (2005); (12) Van Dyk et al. (2006); (13) Van Dyk (2013); (14) Wang et al. (2008); (15) Xu et al. (1994); (16) This paper.

^a Historical extragalactic SNe which have occurred since, and including, SN 1987A.

throughout.

2. *HST* OBSERVATIONS AND PHOTOMETRY

M95 was initially observed by *HST* for LEGUS with WFC3/UVIS on 2014 March 1, however, guide star tracking failed. The galaxy was reobserved on April 23 in bands F275W (total exposure time 2361 s), F336W (1062 s), F438W (908 s), F555W (1062 s), and F814W (908 s). The pointing for the observations was designed intentionally to include the site of SN 2012aw in the total field-of-view. The imaging data were initially run through the standard STScI pipeline procedures for calibration. However, as described in Calzetti et al. (2015), further processing of the ‘flt’ images included a pixel-based correction for the charge transfer efficiency (CTE) losses¹¹. The corrected ‘flc’ images were then combined using the DrizzlePac software (Fruchter et al. 2010; Gonzaga et al. 2012) to produce a distortion-corrected mosaic in each band.

The midpoint of the WFC3 observations was at 2014 April 23 5:28:06, or JD 2456770.7. This is at a SN age of ≈ 768 d, or 2.10 yr.

A three-color-composite image of the light echo is shown in Figure 1. The echo is conspicuously blue, which is not surprising, since we expect dust to scatter preferentially the blue light from the SN. Individual images of the echo are shown for all five bands in Figure 2. The appearance of the echo is more of a circular patch, or blob, and less obviously a single ring. If the echo were a thin ring, though, its profile would be convolved with the WFC3/UVIS PSF and would not be sharply defined. It is also entirely possible that we are actually seeing multiple rings, such as was observed for the interstellar dust-scattered echo around SN 1987A (Crots 1988; see his Figure 1), just not as well resolved. We know that the echo is a recent, post-SN apparition, since no evidence of it exists in the pre-explosion *HST* F555W and F814W images (see Van Dyk et al. 2012, their Figure 1,

¹¹ Anderson, J., 2013, http://www.stsci.edu/hst/wfc3/tools/cte_tools

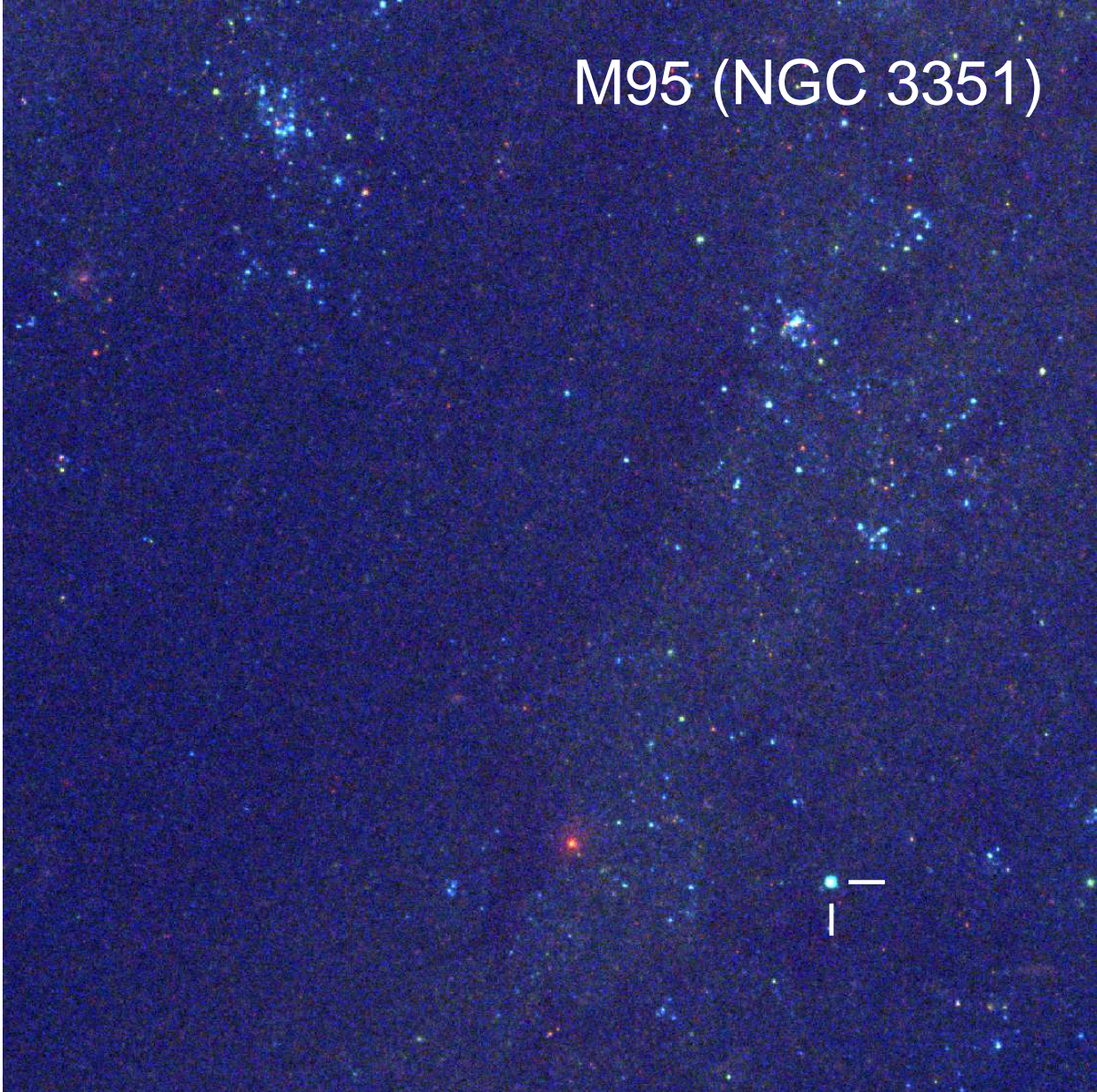


FIG. 1.— A portion of the LEGUS *HST* WFC3/UVIS image mosaics of M95 from 2014 April 23, as a three-color composite of bands F336W, F555W, and F814W. The area shown is $40'' \times 40''$. A prominent light echo is seen at the site of the SN II-P 2012aw, as indicated by the tickmarks. The SN occurred $58''.3$ W and $115''.8$ S of the galactic nucleus. The SN age was ~ 768.2 d, or 2.10 yr, at the time. North is up, and east is to the left.

and Fraser et al. 2012, their Figure 2). Using 20 fiducial stars in common between the pre-SN F814W image and the LEGUS WFC3 F814W image in the immediate SN environment, we can precisely associate the position of the SN progenitor star with the bright spot seen within the echo in Figure 2(e), with a rms uncertainty of $0''.006$ (in right ascension) and $0''.009$ (in declination). There is little question that this is the SN itself, still prominently seen in F814W, relative to the fainter echo brightness. The SN is also apparent in F438W and F555W, but less so in F275W and F336W. A surface brightness enhancement to the southeast along the echo tends to dominate the echo's appearance from F555W blueward.

This implies that the scattering dust is not uniformly distributed, which is consistent with the filamentary nature of interstellar dust and its subsequent effect on the structure of the observed light echoes (e.g., Rest et al. 2011a).

We performed aperture photometry within IRAF¹² of the entire light echo on the drizzled image mosaics in each band, through a range of apertures with increas-

¹² IRAF, the Image Reduction and Analysis Facility is distributed by the National Optical Astronomy Observatory, which is operated by the Association of Universities for Research in Astronomy (AURA) under cooperative agreement with the National Science Foundation (NSF).

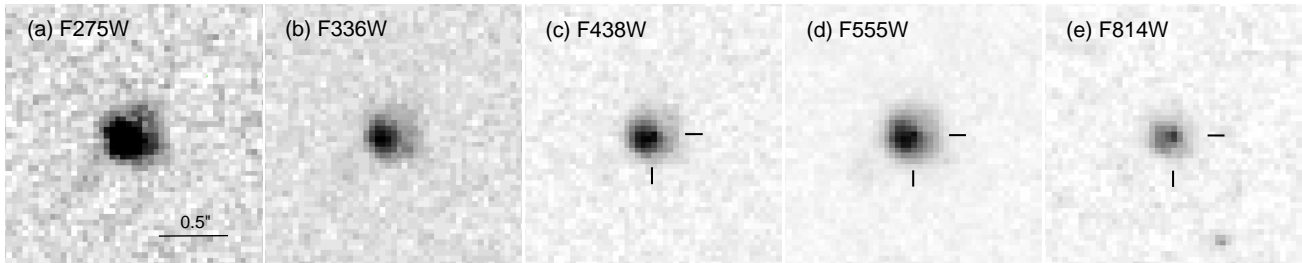


FIG. 2.— A portion of the LEGUS *HST* WFC3/UVIS image mosaics, showing the light echo in more detail, in bands (a) F275W, (b) F336W, (c) F438W, (d) F555W, and (e) F814W. The greyscale has been set to the square-root of the image counts, to enhance the contrast. The SN itself can still be seen, especially in the F438W, F555W, and F814W images, as indicated by the tickmarks. North is up, and east is to the left.

ing radii, in order to estimate the uncertainty in the measurement. A sky annulus was used to estimate the background, which was relatively low in each band. The VEGAMAG zero points for an infinite aperture for the WFC3 bandpasses¹³ were adopted. We list our photometry for the echo in Table 2. The flux of the echo, F_{echo} , which is also listed in the table for each band, was established using these WFC3 zeropoints.

We emphasize that the photometry of the echo in Table 2 actually includes both the echo *and* the SN, particularly at the redder bands. To fully analyze the properties of the echo we needed to remove the SN flux from the total. This was the most complicated step in our analysis and involved significant uncertainty. We started with the three F814W exposures, since the SN was brightest relative to the echo in that band. Even in F814W, though, the emission surrounding the SN is not necessarily spatially flat, so defining a sky background around the point source is nearly impossible. We searched for the location and flux of the SN point source with the understanding that the SN should be the sharpest feature in the image and the nebulous background should be relatively smooth. To this end, we extracted a 19×19 -pixel raster about the target in each flc exposure. We then explored an array of positions and fluxes for the point source. For each trial position and flux, we subtracted the corresponding point-spread function (PSF) from the raw exposures using a library PSF tailored for the particular filter at the particular location in the detector. These library PSFs were constructed from a well-dithered set of data taken of the globular cluster Omega Centauri soon after WFC3 was installed on-board *HST*; they have proven to be good to better than $\sim 2\%$.

We then examined the residuals and identified the optimal location and flux for the SN to be the one that left the post-subtraction residuals as smooth as possible. To evaluate the smoothness of each residual image, we compared that image with a smoothed version of itself. The smoothed version is obtained by convolving the image with a 5×5 quadratic smoothing kernel, which is equivalent to fitting for a six-parameter, two-dimensional quadratic centered on each pixel. In essence, this operation reduces the number of degrees-of-freedom by a factor of $25/6$. The image that was closest to its smoothed version was deemed to be the smoothest. The optimal location and flux of the point source was deemed to be the one that left the image as close as possible to the smooth version of itself.

Using the above strategy, we determined a best-fit location and flux for the SN in each of the F814W flc exposures. When the positions were transformed into the reference frame, they agreed to within a rms uncertainty of 0.09 pixel in x and 0.03 pixel in y . Using this best-fit position, we then found the flux of the point source in each F814W exposure that made the resulting image as smooth as possible and arrived at a flux of $650 \pm 75 e^-$ for an exposure time of 359 s. The PSFs were normalized to correspond to the flux within a 10-pixel aperture, so that is the effective aperture for these measured fluxes. We applied a similar approach to determine a best-fit flux for the SN in each of the other filters ($850 \pm 150 e^-$ in F555W, $400 \pm 45 e^-$ in F438W, $50 \pm 75 e^-$ in F336W, and $100 \pm 50 e^-$ in F275W), using the master-frame position fit from the F814W exposures.

We used the same PSFs to measure fluxes for a number of other isolated point sources in the images, to tie this photometry to the Vega magnitudes for stars in the images produced by Dolphot (Dolphin 2000). The SN flux was then similarly scaled in each band; the resulting magnitudes are listed in Table 2. The uncertainties for the SN magnitudes in each band also include (via quadrature sums) the uncertainties in the scaling, although these are relatively small, compared to the uncertainties due to the smoothed model fitting. Finally, we list in Table 2 the resulting flux, $F_{\text{echo}}^{\text{corr}}$, obtained from subtracting the SN flux from our aperture measurements of the echo flux. The fractional contribution of the SN light to the total echo flux is $\sim 2\%$ in F275W, $\sim 1\%$ in F336W, $\sim 5\%$ in F438W, $\sim 9\%$ in F555W, and $\sim 24\%$ at F814W.

Furthermore, we had $3 \times$ -supersampled and coadded the individual flc exposures in each band, with the SN flux removed, to produce images of just the light echo. In Figure 3 we show the F275W, F438W, and F555W images summed together, in order to increase the overall signal-to-noise ratio of the fainter features of the echo. We did this primarily to reveal any ring-like structure. As one can see, the shape of the echo is still quite patchy and irregular, with the southeast enhancement still dominating the emission, although hints of a ring, or partial arcs, are possibly visible.

3. ANALYSIS OF THE ECHO

As pointed out, it is not clear from Figure 3 that what we are seeing is a well-defined ring, with an expected central void indicating a lack of dust in the plane of the SN. We therefore cannot exclude at this point that the SN is actually immersed in a diffuse dust cloud. Nonetheless, we determined the radius of any ring-like struc-

¹³ http://www.stsci.edu/hst/wfc3/phot_zp_lbn.

TABLE 2
PHOTOMETRY OF SN 2012AW AND ITS LIGHT ECHO^a

Band	m_{echo} (mag)	$F_{\text{echo}}^{\text{corr}}$ (erg cm ⁻² s ⁻¹ Å ⁻¹)	m_{SN} (mag)	$F_{\text{echo}}^{\text{corr}}$ (erg cm ⁻² s ⁻¹ Å ⁻¹)
F275W	21.08 ± 0.02	1.39 ± 0.03 × 10 ⁻¹⁷	25.35 ± 0.61	1.35 ± 0.04 × 10 ⁻¹⁷
F336W	21.28 ± 0.02	1.00 ± 0.02 × 10 ⁻¹⁷	26.12 ± 1.00	9.88 ± 0.03 × 10 ⁻¹⁸
F438W	22.00 ± 0.02	1.06 ± 0.02 × 10 ⁻¹⁷	25.29 ± 0.14	1.01 ± 0.03 × 10 ⁻¹⁷
F555W	21.79 ± 0.01	7.64 ± 0.05 × 10 ⁻¹⁸	24.38 ± 0.20	6.94 ± 0.02 × 10 ⁻¹⁸
F814W	22.26 ± 0.02	1.44 ± 0.03 × 10 ⁻¹⁸	23.79 ± 0.13	1.09 ± 0.01 × 10 ⁻¹⁸

^a We adopted for both F_{echo} and $F_{\text{echo}}^{\text{corr}}$ the WFC3 VEGAMAG flux zero points at http://www.stsci.edu/hst/wfc3/phot_zp_lbn.

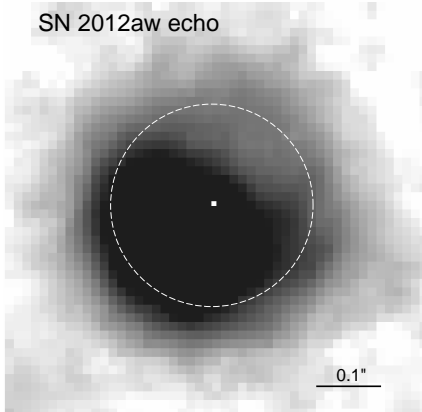


FIG. 3.— A close-up of the SN 2012aw light echo in the sum of images in F275W, F438W, and F555W, after the SN flux had been removed. The images were produced by 3×-supersampling and coadding the individual exposures in each band. The greyscale has been set to the square-root of the image counts, to enhance the contrast. The echo could consist of a ring, or partial arcs, although this is not entirely evident, e.g., there is the surface brightness enhancement seen toward the southeast and no central void indicating a lack of dust in the plane of the SN. Nonetheless, the white circle represents our estimate of a 3.9-pixel ring radius, with a conservative uncertainty of ±0.5 pixel (see Figure 4). The white dot indicates the position of the now-subtracted SN within the echo. At the assumed distance of M95, this corresponds to a radius of 7.6 ± 1.0 pc.

ture by taking cross-cut flux profiles through the echo from its center, avoiding the bright surface brightness enhancement. See Figure 4. We estimated the radius to be 3.9 pixels, with a conservative uncertainty of ±0.5 pixel. At the UVIS plate scale, this radius corresponds to $\theta = 0'.16 \pm 0'.02$. We show our estimate of a ring in Figure 3. We can approximate the light echo ellipsoid as a paraboloid, since the SN's distance from the Earth, D , is so much larger than the geometric dimensions of the echo (e.g., Chevalier 1986; Schaefer 1987). The perpendicular linear distance of the line-of-sight to the SN from the line-of-sight to the echo is $b = D\theta$, where θ is the angular distance between the two lines-of-sight. At the distance D to M95, $b = 7.6 \pm 1.0$ pc.

The distance from the SN to any scattering dust element along the echo, $r = l + ct$, can be obtained from $r^2 = b^2 + l^2$, where l is the distance from the SN to the echo along the line-of-sight (Couderc 1939). For $ct = 0.64$ pc (2.10 ly), we find that $l = 44.1$ pc and $r = 44.7$ pc, with an uncertainty of ±15.0 pc, resulting from the uncertainties in the estimates of both θ and D . The echo is therefore most likely due to interstellar dust.

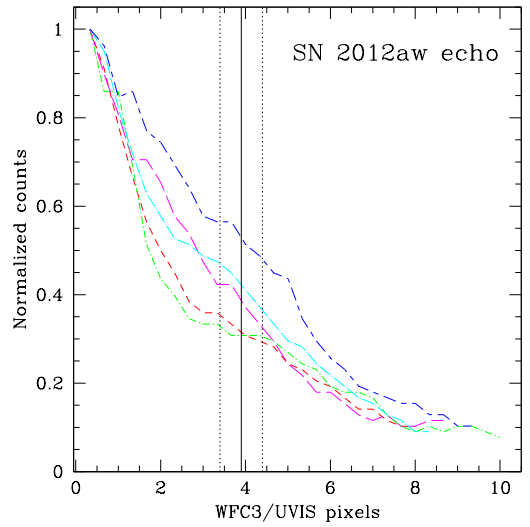


FIG. 4.— Profile cuts through the SN 2012aw light echo, shown in Figure 3, starting at the echo center and progressing toward the north (short-dashed line), northeast (long-dashed line), northwest (dotted short-dashed line), west (dotted long-dashed line), and southwest (short-dashed long-dashed line), intentionally avoiding the bright surface brightness enhancement to the southeast. We estimated from these cuts that the nominal radius of the echo is 3.9 WFC3/UVIS pixels (solid line), with an uncertainty of ±0.5 pixel (dotted line).

We note that much or all of any pre-existing circumstellar dust was likely destroyed by the SN X-ray/UV flash (Van Dyk et al. 2012).

In modeling the echo, even with the uncertainties in the actual distribution of the diffuse interstellar dust, we have assumed that the echo arises from single scattering in a thin dust sheet located between us and the SN, and that the sheet thickness is much smaller than the distance between the sheet and the SN. The scattered flux F at time t from the echo at a given wavelength or bandpass is then

$$F_{\text{echo}}^{\text{corr}}(t) = \int_0^t F_{\text{SN}}(t-t')f(t')dt', \quad (1)$$

where $F_{\text{SN}}(t-t')$ is the fluence of the SN at time $t-t'$, and $f(t')$ is the impulse response function, i.e., the fraction of light scattered by the echo toward us, in units of inverse time, which depends on the nature of the dust and the echo geometry (Chevalier 1986; Cappellaro et al. 2001; Patat 2005). The total SN light is treated as a short pulse over which the SN flux is constant, i.e., $F_{\text{SN}}\Delta t_{\text{SN}} =$

$\int_0^\infty F_{\text{SN}}(t)dt$ (Cappellaro et al. 2001; Patat 2005). The SN fluence is the integral of the light curves in each band with respect to time.

The light curves that we considered here are the combination of those presented in Bose et al. (2013) and Dall’Ora et al. (2014) in *UBVI*, which approximately match what we see from the echo in F336W, F438W, F555W, and F814W, and the *SWIFT* *uvw1* data from Bayless et al. (2013), where *uvw1* is the most similar *SWIFT* bandpass to F275W. See Figure 5. Monitoring in *BVI* began when the SN was at age ≈ 2 days, while the *U* and *uvw1* data commenced at ≈ 4 days. Of course, at the very earliest ages the SN light is dominated by the shock breakout, which is particularly important in the UV as a luminous flash. However, the shock breakout was mostly not observed in the case of SN 2012aw. So, we have simulated what might have occurred, via shock breakout models, specifically, the analytical expressions for RSGs from Nakar & Sari (2010) and the hydrodynamical model for a $13 M_\odot$ RSG from Tominaga et al. (2011). Ehud Nakar graciously provided his algorithms, which we ran assuming an initial mass $M_{\text{ini}} = 12 M_\odot$, a radius¹⁴ $R \approx 750 R_\odot$, and an explosion energy of 10^{51} erg, at the central wavelengths of the five bandpasses. The coefficients in the Nakar & Sari (2010) model have since been calibrated through numerical simulations of the explosion of an analytical star (T. Shussman et al., in preparation), and we used these updates. Nozomu Tominaga also provided us with the output from his RSG model through the five filter bandpasses. We have adjusted this model to $R = 750 R_\odot$ and converted from AB magnitudes to Vega magnitudes.

We show, specifically, the very early-time observed and model UV light curves in Figure 6. Here we are showing the curves in flux units, after reddening correction for an assumed total extinction, $A_V = 0.24$ mag (see below), assuming the Cardelli, Clayton, & Mathis (1989) reddening law with $R_V = 3.1$. The behavior of the two models is relatively similar, although they exhibit notable differences during the first ~ 8 d after explosion. The post-explosion peak of the breakout in the UV is noticeably more pronounced in the Tominaga et al. (2011) model than in the Nakar & Sari (2010) model. The secondary peak at ~ 5 d in the Tominaga et al. model is as luminous, if not somewhat more so, as the initial peak near ~ 0 d. The secondary peak emission for the Nakar & Sari model occurs earlier (at ~ 2.5 d), and is more in line with the first observed datapoint, than for the Tominaga et al. model. These secondary peaks and the declines thereafter undershoot (for Nakar & Sari) and overshoot (for Tominaga et al.) the observed UV light curve. We therefore truncate both model UV curves at ~ 4 d. The behavior of the model light curves, relative to the observations, is quite similar in the other bands, although the initial post-explosion flash diminishes in brightness toward the longer wavelengths. We merely needed to truncate the models before the first datapoint, as we did in the UV, to match the observations in the other bands. The fact that both sets of shock breakout models tend to agree quite well in flux with the early observed data, requiring very little adjustment, implies that the input

¹⁴ Van Dyk et al., in preparation, have also revised the estimated radius of the SN 2012aw progenitor to be $R = 750 R_\odot$.

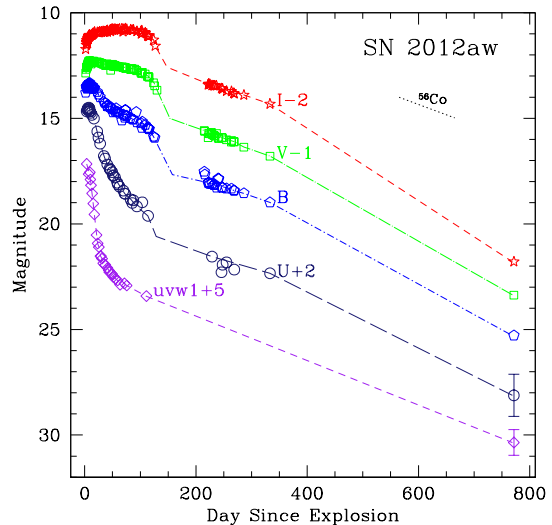


FIG. 5.— Observed light curves (open points) for SN 2012aw from Bayless et al. (2013), Bose et al. (2013) and Dall’Ora et al. (2014) at *SWIFT* *uvw1* (diamonds), *U* (circles), *B* (pentagons), *V* (squares), and *I* (five-pointed stars), which also include our estimate in each band of the SN brightness on day ~ 768 . The lines are interpolations of the observed data points in each band, although we have inserted our best estimate of the plateau end and commencement of the exponential tail to the light curves. Also shown for comparison is the expected decline rate as a result of ^{56}Co decay.

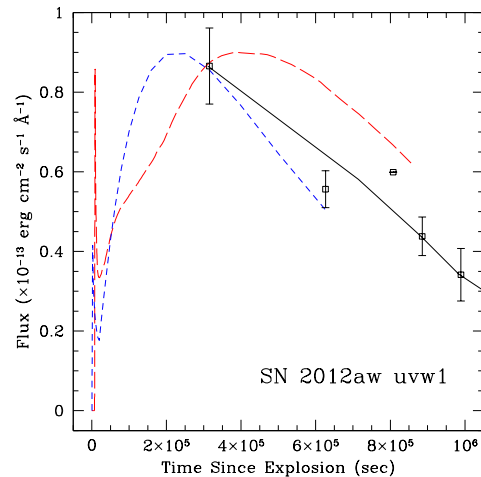


FIG. 6.— Comparison of the *SWIFT* *uvw1* light curve (Bayless et al. 2013) with the adopted shock-breakout flash models in the UV within the first 8.6×10^5 s (~ 10 d). The *SWIFT* data (open squares, solid line) have been reddening-corrected, assuming a total $A_V = 0.24$ mag and the Cardelli, Clayton, & Mathis (1989) reddening law. The short-dashed line is the model light curve using the analytical formulation from Nakar & Sari (2010). The long-dashed line is the model light curve from Tominaga et al. (2011). See the text.

parameters for those models, i.e., the progenitor initial mass and SN explosion energy, are reasonable representations of SN 2012aw and its progenitor star.

We have also included in the observed light curves our estimates of the SN brightness in the 2014 images, as shown in Figure 5, where we assume F275W \sim *uvw1*, F336W \sim *U*, F438W \sim *B*, F555W \sim *V*, and F814W \sim *I*. All of the light curves at late times declined in a manner roughly consistent with radioactive decay from day \sim

TABLE 3
TIME-INTEGRATED SN 2012AW LIGHT CURVES^a

Band	Fluence [no flash] (erg cm ⁻² Å ⁻¹)	Fluence [+Nakar model] (erg cm ⁻² Å ⁻¹)	Fluence [+Tominaga model] (erg cm ⁻² Å ⁻¹)
<i>uvw1</i>	6.79×10^{-8}	9.03×10^{-8}	8.70×10^{-8}
<i>U</i>	1.02×10^{-7}	1.12×10^{-7}	1.12×10^{-7}
<i>B</i>	1.71×10^{-7}	1.72×10^{-7}	1.73×10^{-7}
<i>V</i>	2.06×10^{-7}	2.07×10^{-7}	2.08×10^{-7}
<i>I</i>	1.31×10^{-7}	1.31×10^{-7}	1.31×10^{-7}

^a The conversion from *SWIFT* and Johnson-Cousins Vega magnitudes to flux assumes the following zero points for Vega, as synthesized from the *HST*/STIS calibration spectrum of the star using the package STSDAS/Synphot : 3.99×10^{-9} (*uvw1*), 4.21×10^{-9} (*U*), 6.30×10^{-9} (*B*), 3.61×10^{-9} (*V*), and 1.19×10^{-9} (*I*) erg cm⁻² s⁻¹ Å⁻¹.

340 to day \sim 768, although the *I* curve appears to have declined more steeply, while the *uvw1* curve somewhat less steeply.

After correction for the total extinction to the SN (see below), we integrated, first, just the observed light curves in each band (neglecting the comparatively small uncertainties in the observed SN photometry) and, then, these light curves including the two early-time flash models. Note that for the observed light curves shown in Figure 5 we are missing the end of the plateau in the redder bands. (In the UV no indication exists of a pronounced plateau, so this is not an issue for this band.) For this reason, in particular, we interpolated the light curves in each band from the observed datapoints and estimated the approximate end of the plateau and commencement of the exponential decay phase of the light curves, based on the slope of the decline inferred from the initial data points, post-plateau, and the slope of the data points on the decline after day \sim 200 in each band. The slopes of the decline in the light curves after the end of the observed data (at day \sim 340 in *UBVI*, day \sim 110 in *uvw1*) were interpolated up to our estimates on day \sim 768. Our integrations, then, were over these interpolated light curves, rather than the actual observed data. However, we consider the uncertainties in the total fluence introduced by this assumption to be small, since the behavior of our interpolated light curves are quite similar to that of the observed light curves of the prototypical, normal SN II-P 1999em, for which the end of the plateau was observed; see Hamuy et al. (2001) and Leonard et al. (2002). We adopted Vega as the flux zero point, obtained via synthetic photometry of Vega’s observed *HST* Space Telescope Imaging Spectrograph (STIS) spectrum using STSDAS/SYNPHOT¹⁵ in IRAF. We list the results in Table 3. We see that the flash models in the UV increase the overall fluence by \sim 22% (Tominaga et al. model) to \sim 25% (Nakar & Sari model). This is in better agreement with the observations, since the flux from the echo is relatively high in the UV. The early-time shock-breakout models contribute \sim 9% additional flux at *U*, but only negligible additional amounts at *BVI*.

Treating F_{SN} as the SN maximum flux in each band, we find that the SN pulse duration is 3.8, 21.4, 51.6, 110.3, and 141.2 days in *uvw1*, *U*, *B*, *V*, and *I*, respectively. The maximum value of w , the effective pulse width (Sug-

erman & Crotts 2002; Sugerman 2003), is then \approx 0.7 pc (from *I*). The observed echo thickness, Δb , is unresolved and is conservatively less than the FWHM of a single stellar profile, \lesssim 2.0 WFC3 pixels, or, $\Delta b \lesssim$ 3.9 pc. It follows from Sugerman (2003) that the dust thickness, Δl , is \lesssim 46 pc. This value is clearly not less than our estimate of the dust sheet distance, l . However, since we can only place an upper limit on Δl (given the upper limit on Δb), we infer that its actual value is likely far smaller. Our assumptions for the dust scattering, above, therefore likely still hold.

Following, e.g., Cappellaro et al. (2001) and Patat (2005)

$$f(t) = \frac{cN_H}{r} \Phi(\theta) C_{\text{sca}} \int \phi(a) da, \quad (2)$$

where c is the speed of light, N_H is the H column density, $\Phi(\theta)$ is the scattering “phase function,” C_{sca} is the scattering cross section, and $\phi(a)$ is the grain size distribution for grain radius a . The classical Henyey & Greenstein (1941) $\Phi(\theta)$ is not generally applicable in this case. As Draine (2003) points out, the phase function in the UV is strongly forward-scattering, particularly as the scattering angle becomes small ($\theta \lesssim 10^\circ$). Draine advises tabulating the phase function at short wavelengths, rather than employing an analytical expression. We have adopted his definition of the phase function,

$$\Phi(\theta, \lambda) \equiv \frac{1}{\sigma_{\text{sca}}(\lambda)} \frac{d\sigma_{\text{sca}}(\theta, \lambda)}{d\Omega} \quad (3)$$

where σ_{sca} is the scattering cross section and $d\sigma_{\text{sca}}(\theta, \lambda)/d\Omega$ is the differential scattering cross section per H nucleon, both as a function of wavelength λ . The scattering angle, θ , is obtained from $\cos(\theta) = [(b/ct)^2 - 1]/[(b/ct)^2 + 1]$ (e.g., Schaefer 1987). The scattering angle is therefore $\theta \approx 9.7^\circ$ for the SN 2012aw echo. To compute $\Phi(\theta, \lambda)$ we used the tabulated wavelength-dependent scattering properties for 10° from Draine (2003) for the Weingartner & Draine (2001) Galactic extinction model with $R_V = 3.1$. Furthermore, we also adopted C_{sca} from the Weingartner & Draine dust model, with the update from Draine (2003), which also includes the relevant carbonaceous and silicate grain size distributions ϕ . Van Dyk et al. (2012) argued that the metallicity in the SN environment is consistent with solar metallicity, so assuming a Galactic model for the dust in the SN interstellar environment is probably valid. Fi-

¹⁵ We obtained the *SWIFT* *uvw1* filter transmission function from <http://svo2.cab.inta-csic.es/theory/fps3/>.

nally, we adopted the line-of-sight Galactic foreground visual extinction toward SN 2012aw from Schlafly & Finkbeiner (2011), i.e., $A_V = 0.076$ mag, again, assuming the Cardelli, Clayton, & Mathis (1989) reddening law.

We show the results of our modeling of the echo in Figure 7. The uncertainty in F_{model} shown in the figure is entirely a result of the uncertainty in r , the distance from the SN to any scattering dust element along the echo. Additional uncertainties which we have not included can arise from the scattering dust width, the inclination of the dust sheet with respect to the line-of-sight (Rest et al. 2011a; 2012a), and any asymmetries in the SN explosion (Rest et al. 2011b; Sinnott et al. 2013; early-time spectropolarimetry by Leonard et al. 2012 may have indicated large intrinsic polarization and significant asymmetries in the outer SN ejecta).

The observations constrain N_H in the echo-producing region to a narrow range of $3.55\text{--}3.73 \times 10^{20} \text{ cm}^{-2}$. In Figure 7 we show echo models with the average value, $N_H = 3.6 \times 10^{20} \text{ cm}^{-2}$. Following the relation between N_H and A_V from Güver & Özel (2009), this implies that the internal $A_V = 0.16$ mag for the echo-producing dust. We would obtain the same estimate for A_V based on the relation from Predehl & Schmitt (1995). We note that Van Dyk et al. (2012) estimated the extinction within the host galaxy, based on the equivalent widths of the Na I D features in a high-resolution spectrum of the SN near maximum light, to be $A_V = 0.17 \pm 0.04$ mag (see also Bose et al. 2013), which is consistent with the implied extinction from the echo observations. The SN occurred in a region of M95 seemingly devoid of any recent massive star formation, so natal molecular gas and dust may have already dispersed some time ago. We find the close agreement in these estimates of A_V to be sufficiently reassuring that our light echo models are reasonably correct. If we include the Galactic foreground, the total extinction to SN 2012aw is $A_V = 0.24$ mag.

The echo model is certainly not perfect: We have only included models for the very early-time light curve behavior for the SN and do not know the exact nature of the shock breakout. We employed interpolated light curves in our computation of the SN fluences, since the observed photometric coverage in the five bands is not entirely complete. We also may have incorrectly estimated the SN contribution to the total echo light. Possible faint positive residuals can still be seen in the SN-subtracted images of the echo. Our estimate of the echo radius may well be incorrect. Additionally, our assumed host galaxy distance may not be correct; the NASA/IPAC Extragalactic Database (NED) list 21 Cepheid-based distance moduli which span, to within their uncertainties, a range of about 2.7 Mpc in distance, although the uncertainty-weighted mean of these distance modulus estimates, 29.95 mag, is within the uncertainties of our assumed distance modulus. If the echo radius were actually larger, implying r would also be larger, then N_H (and, thus, A_V) would correspondingly also have to be larger; the dust model itself would also change somewhat, as the scattering angle θ would be decreased. (The reverse would be the case if the echo radius were smaller.) The overall agreement with A_V obtained from the early-time SN spectrum would no longer hold, although it is

conceivable that that estimate is in error. (Dall’Ora et al. 2014 estimated that the host extinction could be as high as $A_V \approx 0.44\text{--}0.59$ mag.) Furthermore, the echo-producing dust in M95 may not be as similar to Milky Way diffuse dust as we have assumed. All of these factors would result in increasing the uncertainty in our overall model.

Nonetheless, we have shown that, to within the uncertainties that we have estimated, we can fully and consistently account for the observed flux from the echo by assuming that the SN light has been scattered by diffuse interstellar dust. The echo light can actually be fit adequately enough without addition of the flash models, although the model flux in the UV is somewhat low. Including the shock breakout flash, using either model, provides a superior representation of the observations in the blue and UV. We know that a flash must occur, so it is logical to have included these models with the observed light curves. All of the echo models tend to overpredict the flux slightly, relative to the observation, at I .

4. CONCLUSIONS

We have discovered in the LEGUS multi-wavelength *HST* imaging a dust-scattered light echo around the SN II-P 2012aw in M95, at ≈ 768 d after explosion. The superior *HST* angular resolution was essential; at $\lesssim 0''.4$ in diameter, observations from the ground under only truly exceptional conditions would have potentially partially resolved the echo. The echo was quite bright at the time, at $\sim 21\text{--}22$ mag in each of the five WFC3/UVIS bands. The echo is a result of the scattering of the total SN light from interstellar dust in the host galaxy, which we assume to have properties similar to Milky Way diffuse dust. In essence, the light echo is a complete record of the SN’s luminosity evolution. We find from comparing a model of the echo to the observations that the amount of the dust extinction in the SN environment responsible for the echo is consistent with the value that was estimated from observations of the SN itself at early times. An independent means of constraining N_H might come from X-ray observations of SN 2012aw: The SN was observed on 2012 April 11 with the *Chandra X-ray Observatory*, and the data provide only a modest constraint, with the value of N_H implied by the echo consistent with the limits allowed by the X-ray spectrum (D. Pooley, private communication).

The echo around SN 2012aw had become detectable in 2014 as the SN light had become sufficiently dim. Under the assumption of a homogeneous thin dust sheet in front of the SN, the light echo is always present and essentially constant in luminosity, even at maximum light, although the echo luminosity is typically ~ 10 mag fainter than the SN at maximum (see, e.g., Patat 2005). If one reasonably assumes that at ~ 768 d the total luminosity is dominated by the echo, it is ~ 11 mag less luminous at V than the SN at maximum light, which is roughly in line with the prediction for typical interstellar light echoes. From the approximations in Patat (2005; his Section 3) and adopting our estimates of the SN-sheet distance and the dust optical depth, one would obtain a SN-light echo contrast of ~ 9 mag. This assumes standard parameters for the dust and a homogeneous distribution within a thin dust sheet — the ~ 2 mag difference between the observed echo brightness and what is predicted could be

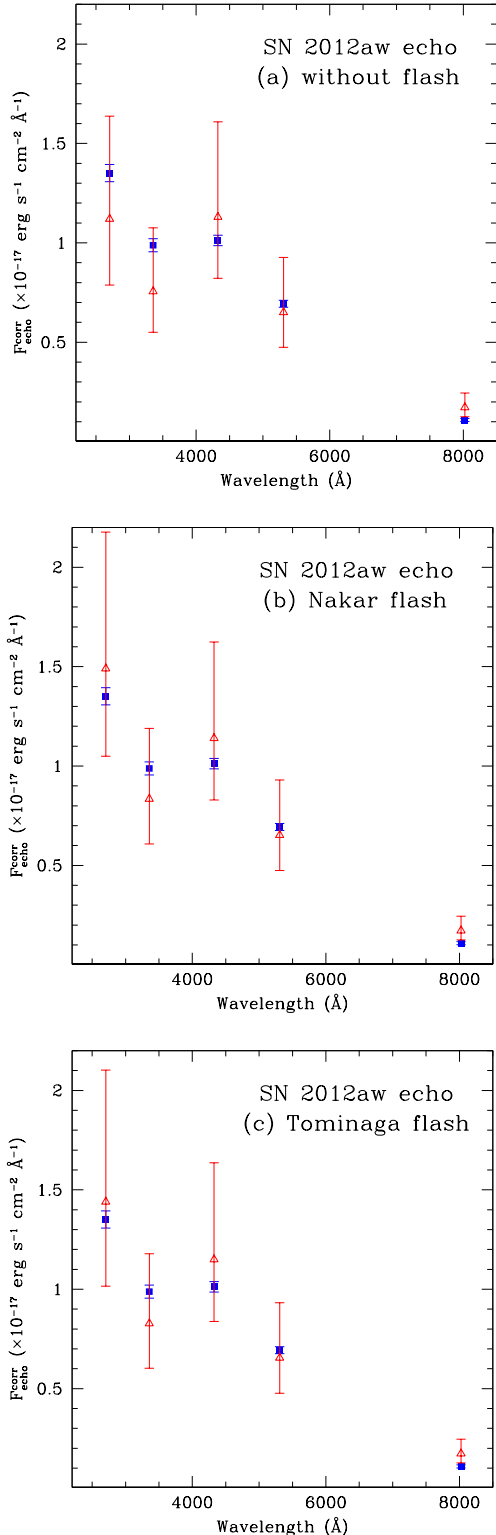


FIG. 7.— The observed light echo flux (solid squares), $F_{\text{echo}}^{\text{corr}}$, in each of the WFC3 bands, after correction for the SN flux, as given in Table 2. Shown for comparison is the model flux (open triangles) as defined in Equations 1 and 2, with an assumed H column density $N_H = 3.6 \times 10^{20}$ cm $^{-2}$ and reddening by the Galactic foreground (Schlafly & Finkbeiner 2011), for (a) the integrated observed light curves with no shock-breakout flash; (b) the integrated observed light curves with the shock breakout flash model from Nakar & Sari (2010); and, (c) the integrated observed light curves with the shock breakout flash model from Tominaga et al. (2011).

explained by an inhomogeneous dust distribution, as apparently indicated by the asymmetric shape of the echo (see Figure 3). One could conclude from the echo’s appearance that there is more dust toward one side of the line-of-sight, so that the echo may also have increased in luminosity with time, as a result of increasing dust optical depth.

Furthermore, we find that, if our estimate of the SN brightness in the F814W band is correct at ≈ 23.8 mag (see Table 2), then the SN at the time was fainter than the observed brightness of the SN progenitor star in that band, 23.39 mag (Van Dyk et al. 2012; Fraser et al. 2012). We cannot completely rule out that dust in the SN ejecta or immediate SN environment is at least partially responsible for the SN’s faintness in 2014. However, it was evident that any circumstellar dust in the progenitor envelope was destroyed by the X-ray/UV flash (Van Dyk et al. 2012). Adopting a SN expansion velocity of 3631 km s $^{-1}$ for SN 2012aw (Bose et al. 2013), after 2.1 yr the SN would have already swept through $\approx 3.4 \times 10^5 R_{\odot}$, or ≈ 1600 AU, most probably beyond the immediate circumstellar environment. Additionally, analysis of *Spitzer Space Telescope* late-time data (to be presented elsewhere) shows that SN 2012aw was fading quite rapidly at 3.6 and 4.5 μm up to day ~ 868 , when emission from the SN in these bands was barely detectable. Dust observed at these wavelengths would be relatively warm, and we cannot discount that colder SN dust may be present. Also, relatively small newly-condensed dust masses have been found for SNe II-P (e.g., Meikle et al. 2007; Kotak et al. 2009; Meikle et al. 2011; although see, e.g., Matsuura et al. 2015 in the case of SN 1987A). A more straightforward conclusion is that the progenitor star has vanished and that the RSG identified by Van Dyk et al. (2012) and Fraser et al. (2012) was almost certainly the progenitor of SN 2012aw.

Finally, the SN 2012aw light echo should be further monitored with *HST*, particularly in the blue, to follow the evolution of its luminosity, as well as potentially to reveal new or evolving echo structures, and better constrain the nature of the echo geometry and of the scattering dust. Continued observations will also place further constraints on the late-time SN brightness and disappearance of the progenitor. Analysis of any future polarimetric imaging of the echo (e.g., Sparks 1994; Sparks et al. 1999), which would allow for an independent distance determination to the host galaxy, however, could be challenging, given the relatively compact nature of the SN 2012aw light echo.

We are grateful for the comments provided by the expert referee, which significantly improved this paper. We appreciate helpful discussions we had with Luc Dessart and the generousities of both Ehud Nakar and Nozomu Tominaga. We also appreciate David Pooley sharing his analysis of the *Chandra* data on SN 2012aw in advance of publication. Based on observations made with the NASA/ESA *Hubble Space Telescope*, obtained at the Space Telescope Science Institute, which is operated by the Association of Universities for Research in Astronomy, Inc., under NASA contract NAS 5-26555. These observations are associated with program #13364. Support for this program was provided by NASA through a

grant from the Space Telescope Science Institute. This research made use of the NASA/IPAC Extragalactic Database (NED), which is operated by the Jet Propulsion Laboratory, California Institute of Technology, under contract with NASA. AH acknowledges funding by

Spanish MINECO under grants AYA2012-39364-C02-01 and SEV 2011-0187-01. SEDM acknowledges support by a Marie Skłodowska-Curie Reintegration Fellowship (H2020-MSCA-IF-2014, project id 661502) awarded by the European Commission.

REFERENCES

- Bayless, A. J., Pritchard, T. A., Roming, P. W. A., et al. 2013, *ApJ*, 764, L13
- Bond, H. E., Gilmozzi, R., Meakes, M. G., et al. 1990, *ApJ*, 354, L49
- Bond, H. E., Henden, A., Levay, Z. G., et al. 2003, *Nature*, 422, 405
- Bose, S., Kumar, B., Sutaria, F., et al. 2013, *MNRAS*, 433, 1871
- Calzetti, D., Lee, J. C., Sabbi, E., et al. 2015, *AJ*, 149, 51
- Cappellaro, E., Patat, F., Mazzali, P. A., et al. 2001, *ApJ*, 549, L215
- Cardelli, J. A., Clayton, G. C., & Mathis, J. S. 1989, *ApJ*, 345, 245
- Chevalier, R. A. 1986, *ApJ*, 308, 225
- Couderc, P. 1939, *Annales d'Astrophysique*, 2, 271
- Crotts, A. P. S. 1988, *ApJ*, 333, L51
- Crotts, A. 2014, *ApJ*, submitted (arXiv:1409.8671)
- Crotts, A. P. S., & Kunkel, W. E. 1991, *ApJ*, 366, L73
- Crotts, A. P. S., Landsman, W. B., Bohlin, R. C., et al. 1992, *ApJ*, 395, L25
- Dall'Orta, M., Botticella, M. T., Pumo, M. L., et al. 2014, *ApJ*, 787, 139
- Dolphin, A. E. 2000, *PASP*, 112, 1383
- Draine, B. T. 2003, *ApJ*, 598, 1017
- Drozhdov, D., Leising, M. D., Milne, P. A., et al. 2014, arXiv:1410.8190
- Ekström, S., Georgy, C., Eggenberger, P., et al. 2012, *A&A*, 537, A146
- Eldridge, J. J., Izzard, R. G., & Tout, C. A. 2008, *MNRAS*, 384, 1109
- Fraser, M., Maund, J. R., Smartt, S. J., et al. 2012, *ApJ*, 759, L13
- Freedman, W. L., Madore, B. F., Gibson, B. K., et al. 2001, *ApJ*, 553, 47
- Fruchter, A. S., et al. 2010, 2010 Space Telescope Science Institute Calibration Workshop, p. 382-387
- Gezari, S., Dessart, L., Basa, S., et al. 2008, *ApJ*, 683, L131
- Gezari, S., Jones, D. O., Sanders, N. E., et al. 2015, *ApJ*, in press (arXiv:1502.06964)
- Gonzaga, S., Hack, W., Fruchter, A., & Mack, J. (eds.) 2012, *The DrizzlePac Handbook* (Baltimore: STScI)
- Gouiffes, C., Rosa, M., Melnick, J., et al. 1988, *A&A*, 198, L9
- Güver, T., & Özel, F. 2009, *MNRAS*, 400, 2050
- Hamuy, M., Pinto, P. A., Maza, J., et al. 2001, *ApJ*, 558, 615
- Heney, L. C., & Greenstein, J. L. 1941, *ApJ*, 93, 70
- Jerkstrand, A., Smartt, S. J., Fraser, M., et al. 2014, *MNRAS*, 439, 3694
- Kapteyn, J. C. 1901, *Astronomische Nachrichten*, 157, 201
- Kochanek, C. S., Khan, R., & Dai, X. 2012, *ApJ*, 759, 20
- Kotak, R., Meikle, W. P. S., Farrah, D., et al. 2009, *ApJ*, 704, 306
- Krause, O., Rieke, G. H., Birkmann, S. M., et al. 2005, *Science*, 308, 1604
- Krause, O., Tanaka, M., Usuda, T., et al. 2008, *Nature*, 456, 617
- Leonard, D. C., Filippenko, A. V., Gates, E. L., et al. 2002, *PASP*, 114, 35
- Leonard, D. C., Pignata, G., Dessart, L., et al. 2012, *The Astronomer's Telegram*, 4033, 1
- Liu, J.-F., Bregman, J. N., & Seitzer, P. 2003, *ApJ*, 582, 919
- Matsuura, M., Dwek, E., Barlow, M. J., et al. 2015, *ApJ*, 800, 50
- Mattila, S., Meikle, W. P. S., Lundqvist, P., et al. 2008, *MNRAS*, 389, 141
- Meikle, W. P. S., Mattila, S., Gerardy, C. L., et al. 2006, *ApJ*, 649, 332
- Meikle, W. P. S., Mattila, S., Pastorello, A., et al. 2007, *ApJ*, 665, 608
- Meikle, W. P. S., Kotak, R., Farrah, D., et al. 2011, *ApJ*, 732, 109
- Miller, A. A., Smith, N., Li, W., et al. 2010, *AJ*, 139, 2218
- Nakar, E., & Sari, R. 2010, *ApJ*, 725, 904
- Patat, F. 2005, *MNRAS*, 357, 1161
- Predehl, P., & Schmitt, J. H. M. M. 1995, *A&A*, 293, 889
- Prieto, J. L., Rest, A., Bianco, F. B., et al. 2014, *ApJ*, 787, LL8
- Quimby, R. M., Wheeler, J. C., Höflich, P., et al. 2007, *ApJ*, 666, 1093
- Quinn, J. L., Garnavich, P. M., Li, W., et al. 2006, *ApJ*, 652, 512
- Rest, A., Suntzeff, N. B., Olsen, K., et al. 2005, *Nature*, 438, 1132
- Rest, A., Matheson, T., Blondin, S., et al. 2008a, *ApJ*, 680, 1137
- Rest, A., Welch, D. L., Suntzeff, N. B., et al. 2008b, *ApJ*, 681, L81
- Rest, A., Sinnott, B., Welch, D. L., et al. 2011a, *ApJ*, 732, 2
- Rest, A., Foley, R. J., Sinnott, B., et al. 2011b, *ApJ*, 732, 3
- Rest, A., Prieto, J. L., Walborn, N. R., et al. 2012a, *Nature*, 482, 375
- Rest, A., Sinnott, B., & Welch, D. L. 2012b, *PASA*, 29, 466
- Ritchey, G. W. 1901, *ApJ*, 14, 293
- Sana, H., de Mink, S. E., de Koter, A., et al. 2012, *Science*, 337, 444
- Schaefer, B. E. 1987, *ApJ*, 323, L47
- Schawinski, K., Justham, S., Wolf, C., et al. 2008, *Science*, 321, 223
- Schlafly, E. F., & Finkbeiner, D. P. 2011, *ApJ*, 737, 103
- Sinnott, B., Welch, D. L., Rest, A., Sutherland, P. G., & Bergmann, M. 2013, *ApJ*, 767, 45
- Sokoloski, J. L., Crotts, A. P. S., Lawrence, S., & Uthas, H. 2013, *ApJ*, 770, L33
- Sparks, W. B. 1994, *ApJ*, 433, 19
- Sparks, W. B. 1996, *ApJ*, 470, 195
- Sparks, W. B., Macchetto, F., Panagia, N., et al. 1999, *ApJ*, 523, 585
- Sugerman, B. E. K. 2003, *AJ*, 126, 1939
- Sugerman, B. E. K. 2005, *ApJ*, 632, L17
- Sugerman, B. E. K., Andrews, J. E., Barlow, M. J., et al. 2012, *ApJ*, 749, 170
- Sugerman, B. E. K., & Crotts, A. P. S. 2002, *ApJ*, 581, L97
- Tamburro, D., Rix, H.-W., Walter, F., et al. 2008, *AJ*, 136, 2872
- Tominaga, N., Morokuma, T., Blinnikov, S. I., et al. 2011, *ApJS*, 193, 20
- Van Dyk, S. D. 2013, *AJ*, 146, 24
- Van Dyk, S. D., Li, W., & Filippenko, A. V. 2006, *PASP*, 118, 351
- Van Dyk, S. D., Cenko, S. B., Poznanski, D., et al. 2012, *ApJ*, 756, 131
- Wang, X., Li, W., Filippenko, A. V., et al. 2008, *ApJ*, 677, 1060
- Weingartner, J. C., & Draine, B. T. 2001, *ApJ*, 548, 29
- Welch, D. L., Clayton, G. C., Campbell, A., et al. 2007, *ApJ*, 669, 525
- Xu, J., Crotts, A. P. S., & Kunkel, W. E. 1994, *ApJ*, 435, 274
- Xu, J., Crotts, A. P. S., & Kunkel, W. E. 1995, *ApJ*, 451, 806 (Erratum: 1996, *ApJ*, 463, 391)
- Yadav, N., Ray, A., Chakraborti, S., et al. 2014, *ApJ*, 782, 30